Coupled Climate Simulation of the Evolution of Global Monsoons in the Holocene*

Z. LIU

Center for Climatic Research, University of Wisconsin—Madison, Madison, Wisconsin

B. OTTO-BLIESNER

National Center for Atmospheric Research,+ Boulder, Colorado

J. KUTZBACH

Center for Climatic Research, University of Wisconsin—Madison, Madison, Wisconsin

L. LI

Earth Environment Institute, Chinese Academy of Sciences, Xi'an, China

C. SHIELDS

National Center for Atmospheric Research,+ Boulder, Colorado

(Manuscript received 10 December 2001, in final form 10 February 2003)

ABSTRACT

Evolution of global monsoons in the Holocene is simulated in a coupled climate model—the Fast Ocean Atmosphere Model—and is also compared with the simulations in another coupled climate model—the NCAR Climate System Model. Holocene climates are simulated under the insolation forcing at 3000, 6000, 8000, and 11 000 years before present. The evolution of six major regional summer monsoons is investigated: the Asian monsoon, the North African monsoon, the North American monsoon, the Australian monsoon, the South American monsoon, and the South African monsoon. Special attention has been paid to the relative roles of the direct insolation forcing and oceanic feedback.

It is found that the responses of the monsoons to the insolation forcing and oceanic feedback differ substantially among regions, because of regional features of atmospheric and oceanic circulation and ocean–atmosphere interaction. In the Northern Hemisphere, the coupled models show a significant enhancement of all of the monsoons in the early Holocene and a gradual weakening toward the present, with the North African monsoon showing the largest relative changes. The monsoons are enhanced in the Holocene by a positive oceanic feedback in North Africa and North America but are suppressed by a negative overall feedback in Asia. In the Southern Hemisphere, monsoons are reduced most significantly in South America, and modestly in South Africa, mainly due to direct insolation forcing. In contrast, the Australian monsoon is enhanced by an overwhelming positive oceanic feedback. The simulated evolution of monsoons during the Holocene shows a general agreement with paleoclimate observations.

1. Introduction

Monsoons are generally characterized by maximum precipitation in summer [June–July–August (JJA)] over the Northern Hemisphere (NH), and in winter [December–January–February (DJF)] over the Southern Hemisphere (SH). Monsoons are critical features of the regional climate in southern and eastern Asia (Webster et al. 1998; Lau et al. 2000), North Africa (e.g., Hastenrath 1994, chapter 6), the American Southwest (Tang and Reiter 1984; Adams and Comrie 1997; Higgins et al. 1997) and Central America (Douglas et al. 1993), northwestern Australia and New Guinea (Suppiah 1992), South America (Zhou and Lau 1998), and South Africa (e.g., Hastenrath 1994, chapter 6). (Hereafter, for convenience, these six monsoons will be called the Asian monsoon, the North African monsoon, the North American monsoon, the Australian monsoon, the South American monsoon, and the South African monsoon.)

Paleoclimate records suggest that these regional monsoons have undergone significant changes in the Holocene (about the last 10 000 years). Most notable are

* Center for Climate Research Contribution Number 775.

+ The National Center for Atmospheric Research is sponsored by the National Science Foundation.

Corresponding author address: Dr. Z. Liu, Center for Climatic Research, 1225 W. Dayton St., Madison, WI 53706-1695.
E-mail: zliu3@facstaff.wisc.edu

the monsoon expansions in the early to mid-Holocene in North Africa and Asia (e.g., Street-Perrott and Perrott 1993; Kutzbach and Street-Perrott 1985; Winkler and Wang 1993; Kohfeld and Harrison 2000). Substantial monsoon changes have also been recorded over the American Southwest (Thompson et al. 1993; Webb et al. 1993; Harrison et al. 2003) and Central America (Metcalfe et al. 2000; Markgraf et al. 2000), South America (Markgraf 1993; Betancourt 2000; Maslin and Burns, 2000), and northwestern Australia and New Guinea (Harrison and Dodson 1993; Johnson et al. 1999; Wyrwoll and Miller 2001). The extent of the monsoon changes and even the sign of the changes, however, vary substantially from region to region. Among the three NH monsoons, the North African monsoon exhibits the most dramatic changes. In the SH, the South American monsoon is clearly reduced, while the Australian monsoon seems to be enhanced relative to the present. The reasons for this wide range of monsoon changes remain not well understood.

Earlier modeling studies of the Holocene monsoon focused on the effect of direct insolation forcing on the North African–Asian monsoons (e.g., Kutzbach and Otto-Bliesner 1982; Kutzbach and Guetter 1986; Mitchell et al. 1988; Joussaume et al. 1999; Otto-Bliesner 1999). These studies show that the enhanced seasonal cycle of the NH insolation in the early to mid-Holocene increases the land–sea surface temperature contrast in summer and, in turn, monsoon activity. Over North Africa, this orbitally forced monsoon enhancement is further amplified by land-surface (Kutzbach et al. 1996; Texier et al. 1997; Doherty et al. 2000) and oceanic (Kutzbach and Liu 1997; Hewitt and Mitchell 1998; Braconnot et al. 2000) feedbacks. Many important questions remain open, especially for monsoons outside of the North African–Asian region. The mechanism for the evolution of the Australian monsoon is not understood. Even with a reduced seasonal insolation in the SH, the observed Australian monsoon seems to be enhanced in the early to mid-Holocene (Johnson et al. 1999; Wyrwoll and Miller 2001); this monsoon enhancement is opposite to the monsonal response found in previous AGCM simulations (Kutzbach and Guetter 1986; Mitchell et al. 1988) and cannot be explained by the direct insolation forcing alone. The role of oceanic feedback on Holocene monsoons remains poorly understood. Relative to the glacial times, the change of SST is small in the Holocene (about 1°C in the Tropics), such that even with the SST prescribed the same as the present, early AGCM simulations achieved some successes for the North African–Asian monsoons (e.g., Kutzbach and Otto-Bliesner 1982). However, this small SST anomaly may still have significant impact on regional monsoons in the Holocene, because these SST changes occur in large areas in the Tropics that may generate substantial forcing to the atmospheric circulation.

Here, we will mainly discuss the Holocene climate simulations at the time slices of 11 000, 8000, 6000, and 3000 years before present, hereafter abbreviated as 11, 8, 6 and 3 kyr BP, in a fully coupled climate model: the Fast Ocean Atmosphere Model (FOAM_1.0; Jacob 1997). We will focus on the evolution of these regional monsoons and their mechanisms, especially those associated with oceanic feedbacks. The coupled model is described in section 2 and the coupled simulations in section 3. The forcing mechanisms underlying regional monsoon responses are further examined in section 4. A synthesis of major monsoon changes is given in section 5 and a brief comparison with published paleoclimate records is presented in section 6. A summary is given in section 7. Finally, to assess the sensitivity of our model results, major features of the Holocene FOAM simulations are compared briefly in the appendix with another fully coupled climate model—the National Center for Atmospheric Research (NCAR) Climate System Model (CSM; Otto-Bliesner and Brady 2001).

This paper is a part of our overall effort toward the understanding of the evolution of Holocene climate. This paper focuses on the synthesis of the monsoon evolution and the comparison of different regional monsoons. More detailed studies on other aspects of the results are discussed in several related papers: Harrison et al. (2003) and Liu et al. (2002, manuscript submitted to *Climate Dyn.*, hereafter L02) on the mechanism and model–data comparisons of the 6-kyr monsoon changes for the North American monsoon and global monsoons, respectively, and Liu et al. (2003) for the evolution of the upper ocean during the Holocene.

2. Model

FOAM is a fully coupled ocean–atmosphere model without flux adjustment. The atmospheric component of FOAM is a fully parallel version of the NCAR CCM2, in which the atmospheric physics is replaced by those of CCM3 (Jacob 1997). This component has R15 resolution (equivalent grid spacing about 7.5° long, 4° lat). The ocean component was developed following the Geophysical Fluid Dynamics Laboratory Modular Ocean Model (GFDL MOM) with a resolution of 1.4° latitude, 2.8° longitude, 16 levels. All the coupled FOAM simulations are integrated for 150 yr starting from the 600th year of a long modern control run. The upper ocean and the atmosphere reach quasi equilibrium in the first several decades; the data of the last 120 yr are used to construct the monthly climatology here.

FOAM captures most major features of the observed tropical climatology (Jacob 1997). Figure 1 presents the climatological surface air temperature for boreal summer (Fig. 1a) and winter (Fig. 1d) in the modern control run (F0k), which resembles broadly the climatology of the standard version of the NCAR CSM (Boville and Gent 1998). In boreal summer, the precipitation belt is dominated by the intertropical convergence zone (ITCZ) over the ocean north of the equator (Fig. 1b). Substantial precipitation penetrates deep into the middle of the

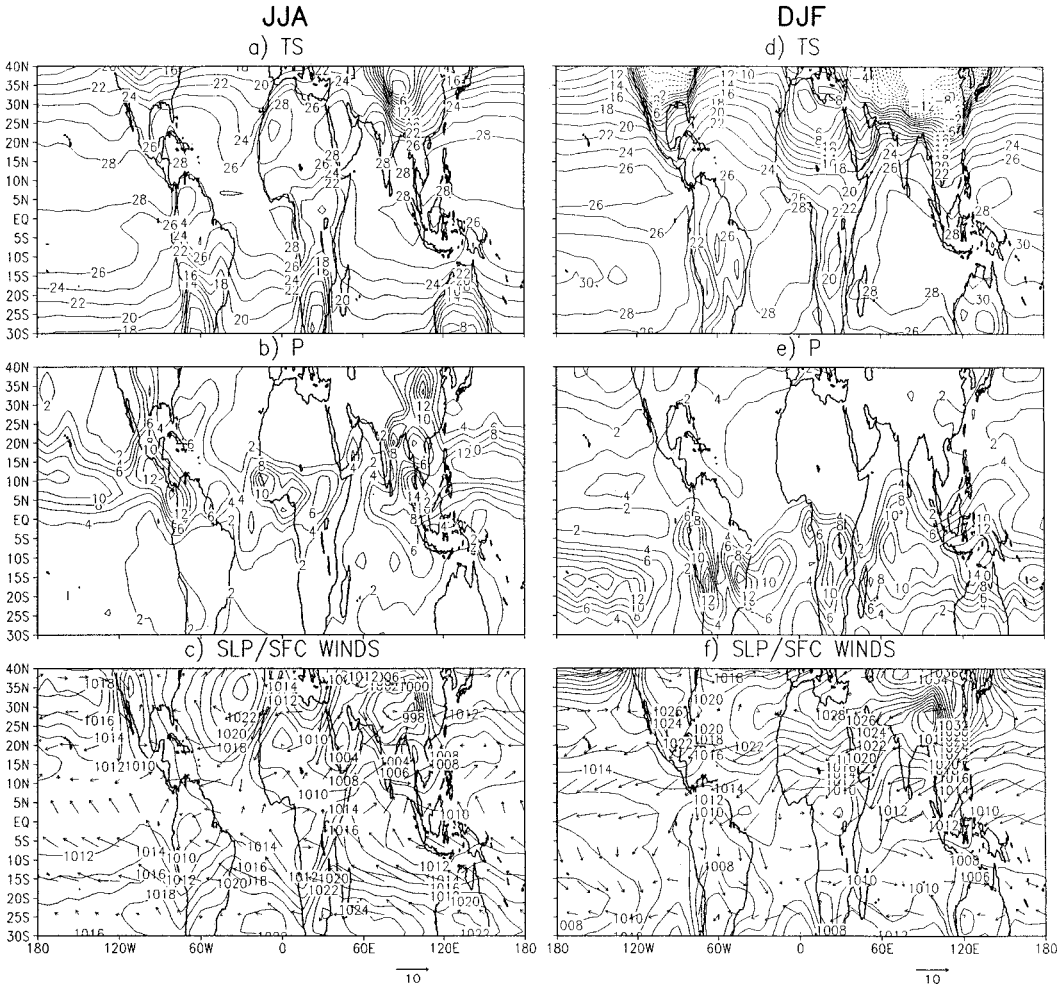

FIG. 1. Simulated climatology of the FOAM control run (F0k) for boreal summer (JJA) (a) surface air temperature, (b) precipitation, (c) sea level pressure and surface winds; and boreal winter (DJF) (d) surface air temperature, (e) precipitation, (f) sea level pressure and surface winds (m s^{-1}). The contour intervals are 2°C for temperature, 2 mm day^{-1} for precipitation, and 2 mb for pressure.

Asian and North American continents. A strong surface low pressure center develops over the region of southern and eastern Asia (Fig. 1c). This surface Asian low (Fig. 1c) extends westward across northern Africa at about 20°N to form a part of the northern African monsoon. A surface low pressure center also develops over the American Southwest–Mexico region (Fig. 1c), forming a part of the North American monsoon (Adams and Comrie 1997). These surface low pressure systems are accompanied by substantial southwesterly monsoon winds (Fig. 1c) and heavy precipitations (Fig. 1b), especially in North Africa and southern and eastern Asia. In austral summer, the precipitation belt associated with the ITCZ migrates into the SH (Fig. 1e). (As in almost all the coupled models, FOAM tends to produce a double ITCZ.) A surface low pressure center develops over northern Australia (Fig. 1f). The intensive winter Siberian high drives a strong southward Asian winter monsoon wind, which veers southeastward after crossing the equator, converging toward northwestern Australia–New Guinea (Fig. 1f). Two surface low pressure centers also develop over South America and central southern Africa (Fig. 1f), associated with the monsoon circulations there.

3. Monsoon evolution in the Holocene

Four coupled Holocene simulations are performed with the same setting as the FOAM control run, except that the insolation forcings are set at 3, 6, 8, and 11 kyr (Berger 1978) for the F3k, F6k, F8k, and F11k runs, respectively. In all of the experiments, the continental ice sheets and the land vegetation are kept at the present conditions and the atmospheric CO_2 concentration is prescribed at the present level of 330 ppmv.

The dominant insolation forcing in the early to mid-Holocene is an increased seasonal cycle in the NH and a decreased seasonal cycle in the SH. This change of

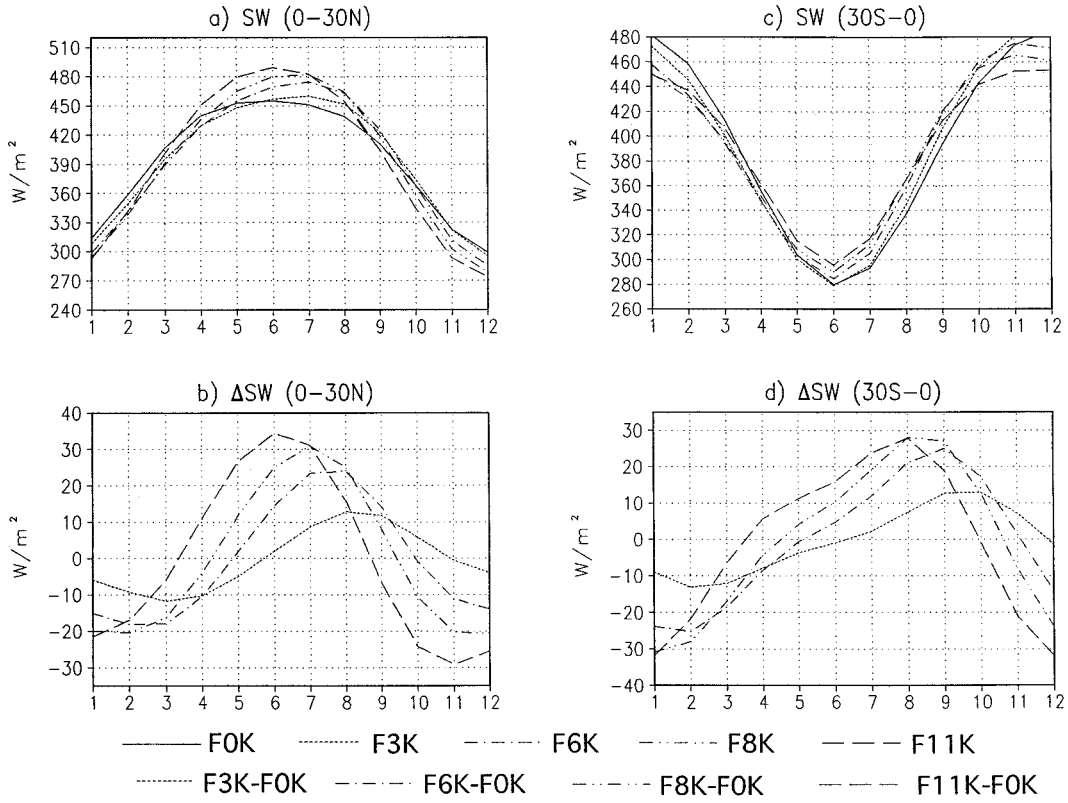

FIG. 2. Monthly evolution of solar radiation at 0, 3, 6, 8, and 11 kyr. The insolation (W m^{-2}) averaged for 0°–30°N is shown (a) for the total and (b) for the anomaly from the present, while the insolation averaged for 30°S–0° is shown (c) for the total and (d) for the anomaly from the present.

seasonal orbital forcing is mainly caused by the 21 000-yr precession cycle, in which the perihelion changes from January at present to November at 3 kyr, September at 6 kyr, August at 8 kyr, and June at 11 kyr. As a result, maximum summer insolation decreases toward the present in the NH but increases in the SH (Figs. 2a,c). With this direct insolation forcing, one should generally expect a maximum (minimum) NH (SH) monsoon at 11 kyr, and a gradual weakening (strengthening) of the summer NH (SH) monsoons as one proceeds to 8, 6, 3, and 0 kyr, as shown in previous AGCM and coupled AGCM–slab ocean simulations (Kutzbach and Street-Perrott 1985; Kutzbach and Guetter 1986; COHMAP Members 1988; Kutzbach et al. 1998). In the following, we will first study the early Holocene at 11 kyr, and then the evolution of monsoon toward the present.[1]

a. Early Holocene monsoon

The response of the NH monsoons at 11 kyr can be seen in the difference between F11k and F0k for boreal summer (JJA) surface air temperature (Fig. 3a), precipitation (Fig. 3b), and sea level pressure and surface winds (Fig. 3c). Surface air warms over Asia, North Africa, and North America in response to the increased summer insolation, but cools slightly in tropical North Africa due to the increased cloudiness (Fig. 3a). A low surface pressure anomaly develops across South Asia–East Asia and North Africa (Fig. 3c). A secondary low pressure anomaly is established over the American Southwest. These negative sea level pressure anomalies are accompanied by an increase of upstream southwesterly monsoon winds (Fig. 3c) and local precipitation (Fig. 3b). A belt of increased precipitation stretches from central China southwestward, through southern Asia, into the African sub-Saharan region (Fig. 3b). The zone of increased precipitation in America extends from Central America northwestward, through Mexico, into the American Southwest. This increase of summer rainfall is accompanied by an arc-shaped region of reduced precipitation in the United States stretching from the northwest Pacific coast to the southeast Atlantic coast (Fig. 3b; Harrison et al. 2003).

The reduction of summer (DJF) insolation in the SH leads to a decrease in land–sea temperature contrast and weaker monsoons over South America and South Africa (Figs. 3d–f). Anomalous surface low pressure centers

[1] Our monthly averages use the present-day calendar month. Kutzbach and Gallimore (1988) have shown that a proper celestial longitude average can account for the varying lengths of seasons. The results of celestial longitude averages are not presented here because the differences, while detectable, do not change our primary conclusions.

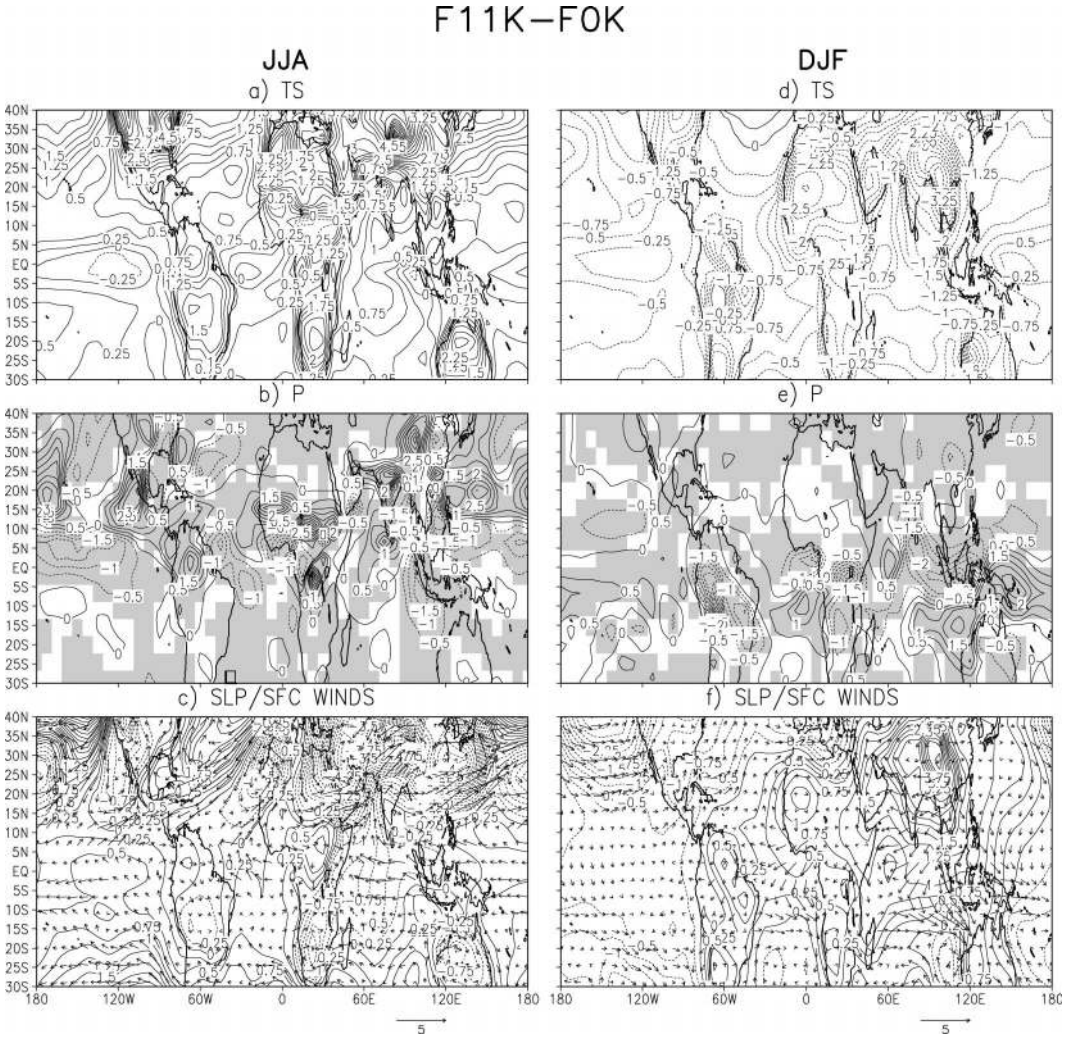

FIG. 3. Patterns of climate anomalies at 11 kyr simulated in FOAM. The figure is arranged the same as Fig. 1, but for the difference F11ka − F0k. Contour intervals are 0.25°C for temperature, 0.5 mm day^{-1} for precipitation, and 0.25 mb for pressure; surface winds are in m s^{-1}. Areas with statistical significance higher than 95% are shaded for the precipitation.

develop over the eastern subtropical Pacific and Atlantic (Fig. 3f), increasing precipitations there (Fig. 3e). In contrast, monsoon rainfall over northwestern Australia–New Guinea is increased (Fig. 3e) and is accompanied by an anomalous low pressure center just offshore of western Australia and a stronger northwesterly monsoon wind (Fig. 3f).

Some broad features of the simulated monsoon responses are in qualitative agreement with previous AGCM studies, such as the enhanced African–Asian monsoon and the North American monsoon, and the reduced South American and South African monsoon (Kutzbach and Otto-Bliesner 1982; Kutzbach and Guetter 1986; Kutzbach et al. 1998). There are, however, important differences from the previous studies. Previous AGCM experiments have shown a rather limited expansion of the North African monsoon and all of the AGCM experiments have shown a decreased monsoonal precipitation over the northwestern Australia.

b. Monsoon evolution in the Holocene

Throughout the early to mid-Holocene, major features of the monsoon responses remain qualitatively similar, but the magnitude and extent of the responses vary significantly with time. In the late Holocene (3 kyr), the monsoon responses are generally small and less significant. (All of the major features discussed below are statistically significant at 95% level, except at 3 kyr.) Figure 4 illustrates the seasonal cycle of the precipitation anomaly for the Asian monsoon (10°–40°N, 60°–120°E), the North African monsoon (5°–30°N, 20°W–30°E), the North American monsoon (0°–40°N, 110°–60°W), the Australian monsoon (20°S–0°, 110°–150°E),

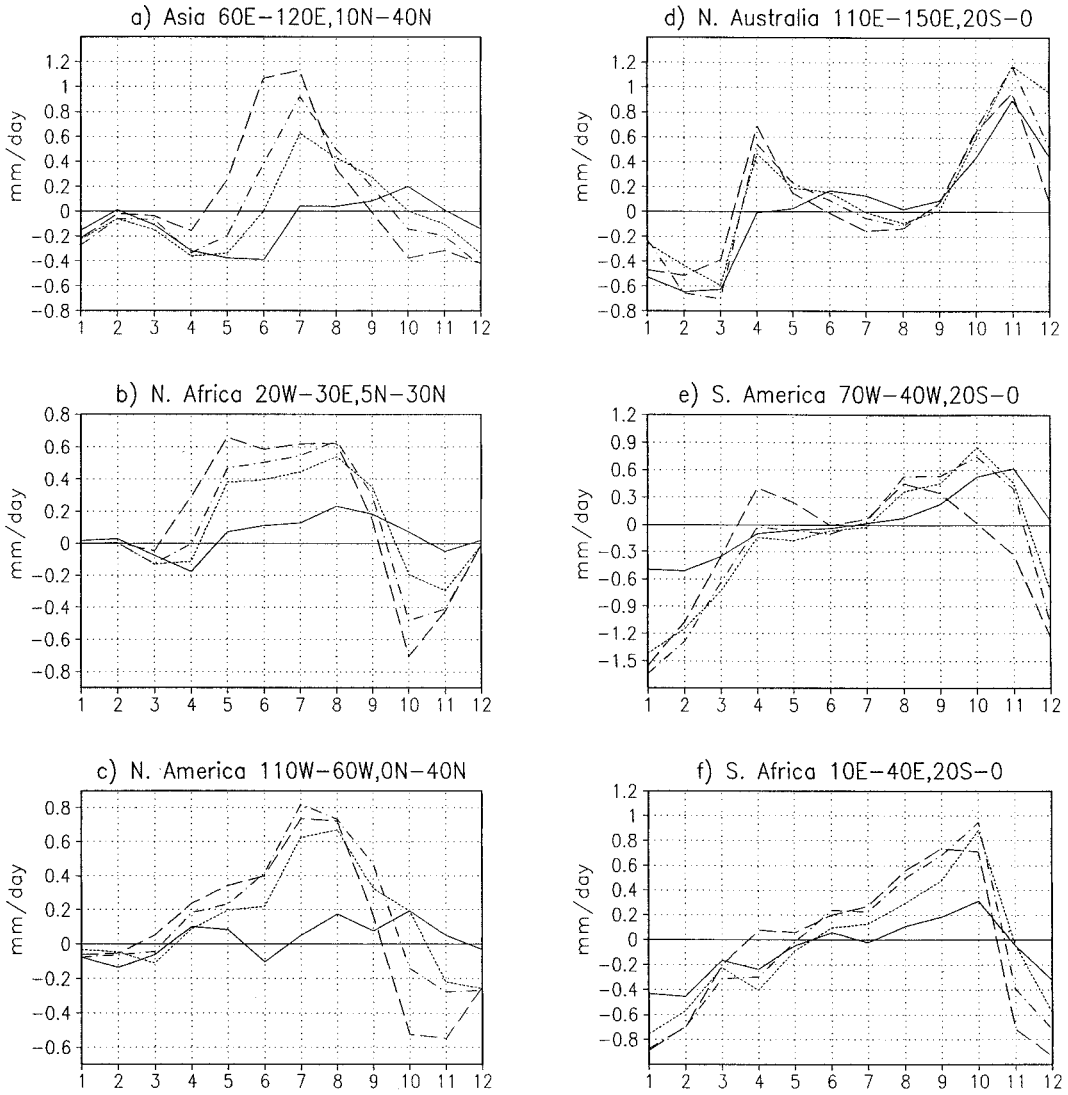

FIG. 4. Monthly evolution of land precipitation anomalies from the present at 3 (solid), 6 (dot), 8 (dash–dot), and 11 kyr (dash) in FOAM averaged for the (a) Asian (10°–40°N, 60°–120°E), (b) North African (5°–30°N, 20°W–30°E), (c) North American (0°–40°N, 120°–60°W), (d) Australian (20°S–0°, 110°–150°E), (e) South American (20°S–0°, 70°–40°W), and (f) South African (20°S–0°, 10°–40°E) monsoons.

the South American monsoon (20°S–0°, 70°–40°W), and the South African monsoon (20°S–0°, 10°–40°E). For the North African monsoon, the precipitation anomaly in May–September decreases modestly from the early (11 kyr) to mid-Holocene (6 kyr), and then disappears toward the late Holocene (3 kyr; Fig. 4b). The decrease of enhanced summer rainfall is about twice as fast between 6 and 3 kyr as between 11 and 6 kyr; this follows the summer insolation anomaly (Fig. 2b), which shows a difference of the peak values that is about twice as large for 6–0 kyr as for 11–6 kyr. The expanded rainfall anomaly pattern shifts from 11 kyr southward, first modestly to 8 and 6 kyr, and then significantly to 3 kyr (Figs. 3b, 5e,c,a), with the shift most clearly seen in the tropical western Africa, where the positive rainfall anomaly belt south of the Sahel (at 15°N) is accompanied by a negative belt to the south (at 5°N). Although it appears to follow the insolation almost linearly, the North African monsoon, as will be shown later (section 4), is enhanced not only by the direct radiation forcing, but also by a positive oceanic feedback.

Summer precipitation of Asian monsoon is also intensified relative to the present (Fig. 4a), with a significant increase occurring from 11 to 6 kyr. From 11 to 6 kyr, summer rainfall is increased substantially from northern India to central and western China (Figs. 5c,e and 3b), representing a significant enhancement of the Asian monsoon. However, rainfall is reduced modestly in regions near the east coast of China and India (Figs. 5c,e and 3b). The more complex pattern of precipitation

change in Asia, relative to North Africa, implies a stronger heterogeneity of monsoon dynamics in the former, consistent with our present understanding of the dynamics of the Asian monsoon (Lau et al. 2000). Furthermore, as will be seen later (section 4), the somewhat complex response of the Asian monsoon is also related to a negative feedback from the ocean.

The North American monsoon is also increased compared with the present in the early Holocene. This enhancement decreases toward the late Holocene, especially between 6 and 3 kyr (Fig. 4c). The largest increases in rainfall occur over Central America and the northernmost part of South America (Figs. 5a,c,e and 3b). In the American Southwest, summer rainfall also increases in a north–south band near 110°E (the southern portion of the Colorado plateau), which is sandwiched between negative rainfall anomalies on the northwest and the southeast coasts of the United States. The dry arc is caused by descending flow that compensates for the ascending flow in the region of increased monsoon over the Colorado plateau [see Harrison et al. (2003) for more details]. This increase of the North American monsoon is due to both the direct solar radiation forcing and oceanic feedback, somewhat similar to North Africa, as will be discussed later.

In the SH, the evolutions of seasonal rainfall over South America (Fig. 4e) and South Africa (Fig. 4f) are similar, both experiencing a modest reduction of rainfall in austral summer and an earlier onset of monsoon rainfall in late spring during the Holocene. Except in some coastal regions, the reductions of the summer precipitation are continental-wide over the Amazon basin and over the tropical forests in South Africa (Figs. 5b,d,f and 3e). In contrast, the Australian monsoon is increased from austral late spring to early summer (Fig. 4d) throughout the Holocene. The summer precipitation shows a persistent pattern of positive anomalies extending from the tropical South Indian Ocean into the northwestern Australian continent (Figs. 5b,d,f and 3e). This enhancement of the Australian monsoon, opposite to the effect expected from the local insolation (Figs. 2c,d), will be shown later to be dominated by an oceanic feedback there.

4. Effects of direct insolation and oceanic feedback

In the fully coupled model discussed above, the monsoon response is caused by both the effects of the direct insolation forcing and oceanic feedback. One convenient way (Kutzbach and Liu 1997; Hewitt and Mitchell 1998; Braconnot et al. 2000) of separating the two effects is to decompose the total response (coupled Holocene run minus the modern control run) into the direct insolation (fixed modern SST run minus control run) and oceanic feedback (coupled Holocene run minus the fixed modern SST run). Here, the fixed SST run is an AGCM experiment in which the SST is prescribed the same as the seasonal climatology of the modern control run. (This broad definition of ''oceanic feedback'' includes both the thermodynamic and dynamic effects of the oceanic response.) Therefore, four fixed SST experiments—F3kFix F6kFix, F8kFix, and F11kFix—are carried out using the AGCM component of FOAM: these fixed SST AGCM experiments are identical to the coupled experiments F3k, F6k, F8k, and F11k, respectively, except that the SST is prescribed as the seasonal climatology of the modern control. These fixed SST experiments are integrated for 15 yr, with the last 10 yr being used for the monthly climatology.

It is helpful to first consider the effects of direct insolation and oceanic feedback for an idealized monsoon response. With an insolation heating anomaly, both the land and ocean will be warmed, with the former more than the latter. The warming over land alone (direct insolation effect) intensifies the monsoon, while the warming over the ocean alone (oceanic feedback) tends to weaken the monsoon. The net effect is a stronger monsoon because the land warms more than the ocean. In this idealized scenario, hereafter referred to the canonical Holocene monsoon response, the NH (SH) monsoon is enhanced (reduced) in the coupled model in the Holocene in boreal (austral) summer, but with a magnitude smaller than that generated in the fixed SST simulation because the oceanic feedback is always negative, opposing the monsoon change that is forced by the direct insolation forcing. Therefore, the monsoon sensitivity to orbital forcing is always weaker in a coupled simulation than in the corresponding fixed SST AGCM simulation. This canonical monsoon response has been used previously as a basis for the understanding of Holocene monsoon responses in AGCMs and coupled AGCM–slab ocean models (Kutzbach and Webb 1993). However, as will be seen below, with the fully coupled ocean–atmosphere model, the dynamics of the atmospheric and oceanic circulation can generate strong regional features that alter the monsoon response significantly from the canonical response. Although the rest of the section focuses on the 11 kyr, all of the discussion can be applied to other Holocene times, qualitatively.

a. North African and Asian monsoons

The direct radiation effect at 11 ka intensifies the summer monsoon winds and precipitation in both North Africa and South Asia–East Asia (Figs. 6a–c), consistent with previous AGCM experiments (e.g., Kutzbach and Otto-Bliesner 1982; Kutzbach and Guetter 1986; Mitchell et al. 1988). The oceanic feedback, however, is more complicated than in the canonical response. For the North African monsoon, the ocean exerts a positive feedback on the monsoon rainfall (Figs. 7b,c). The zonal band of positive rainfall anomaly near 15°N is accompanied by a negative band of comparable strength to the south near 5°N (Fig. 7b). This implies that, rather than increasing the total amount of monsoon rainfall, the ocean mainly acts to shift the monsoon rainfall farther

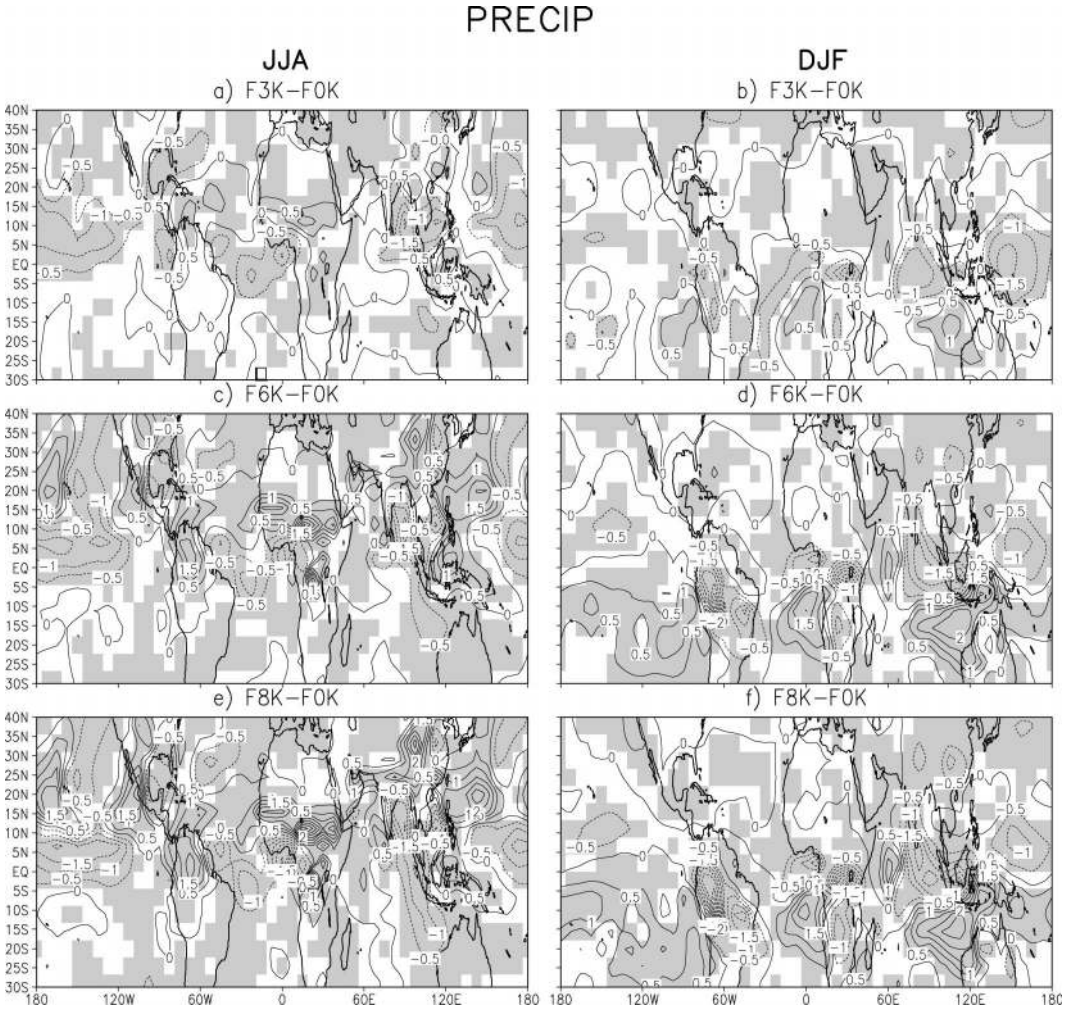

FIG. 5. Patterns of the precipitation anomaly from the present simulated in FOAM for boreal summer and winter at (a), (b) 3 kyr (F3k − F0k), (c), (d) 6 kyr (F6k − F0k), (e), (f) and 8 kyr (F8k − F0k). The contour interval is 0.5 mm day^{-1}. The corresponding precipitation figures for 11 kyr are shown in Figs. 3b,e. Areas with statistical significance higher than 95% are shaded.

northward toward the Sahel. The northward expansion of the North African monsoon is forced by a northward anomalous SST gradient in the tropical Atlantic (Fig. 8g), which causes the ITCZ to migrate northward and allows Atlantic moisture to penetrate farther inland. The northward SST gradient is generated partly by an early summer insolation heating anomaly that is stronger in the NH than in the SH (Figs. 2b,d) and partly by a wind–evaporation feedback that is triggered by the monsoon intensification over North Africa (Kutzbach and Liu 1997).

For the Asian monsoon, the overall oceanic feedback appears to be negative as in the canonical response, but with some regional differences. Over most of southern and eastern Asia, oceanic feedback reduces summer rainfall (Fig. 7b), counteracting the direct radiation effect (Fig. 6b). The total monsoon response is dominated by the direct insolation heating over land, with the rainfall increased over most of the monsoon region (Fig. 3b). Overall, the reduced land precipitation seems to be related to the warm SST anomalies over the western and tropical western North Pacific (Fig. 8g). These warm SST anomalies induce strong moisture convergence over the ocean (Figs. 7b,c), reducing the moisture convergence and, in turn, precipitation over the land (Liu et al. 1999). In small regions of eastern China and southeastern India, the rainfall reduction by the ocean feedback is so strong that the net summer rainfall is reduced there (Fig. 3b). This strong negative oceanic feedback contributes to an inhomogeneous monsoon response in Asia.

b. North American monsoon

The response of the North American monsoon and the associated oceanic feedback in the early Holocene

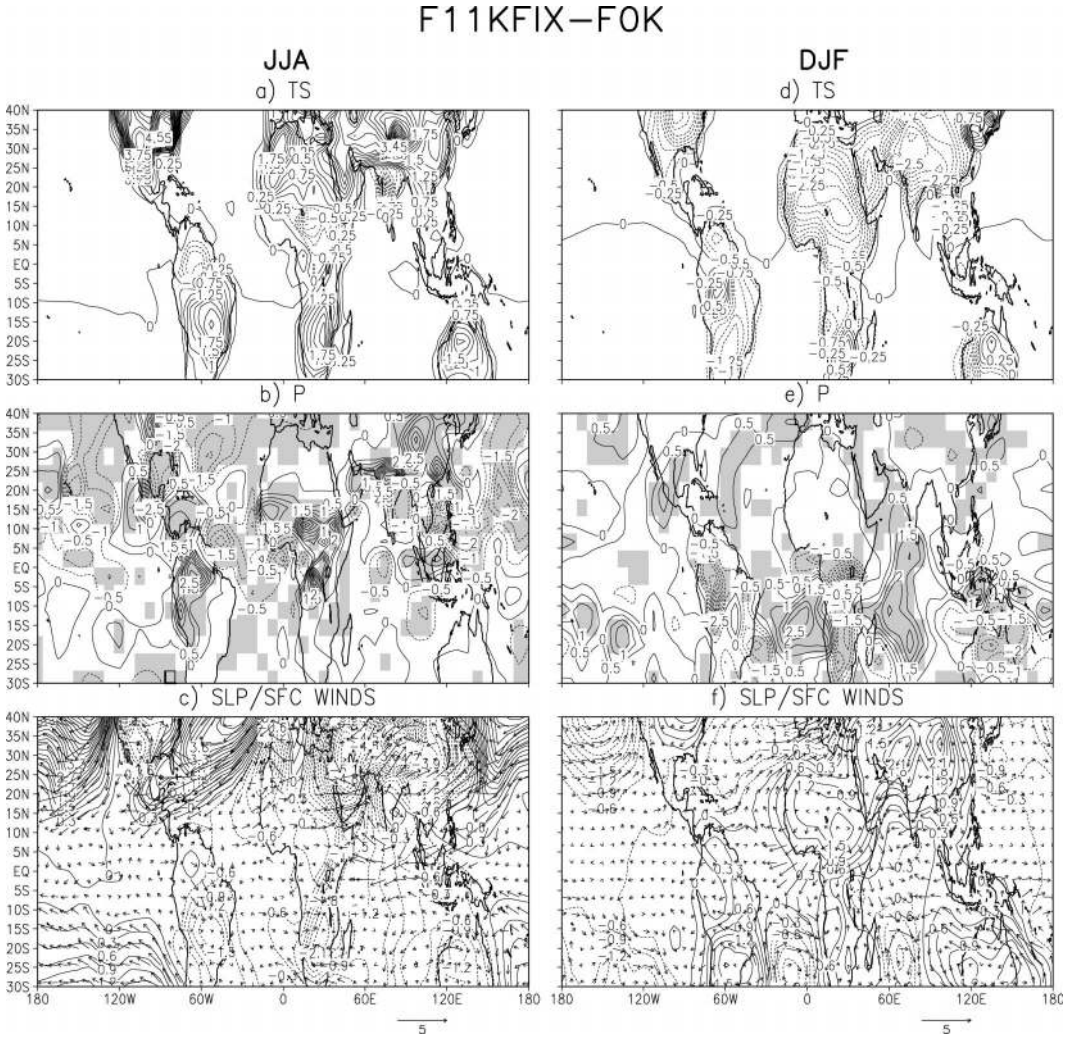

FIG. 6. Direct radiation effect on climate at 11 kyr as simulated from F11kFix − F0k. Plots and units are the same as in Fig. 3. Areas with statistical significance higher than 95% are shaded for the precipitation.

are somewhat similar to the North African monsoon [see Harrison et al. (2003) for more details]. The anomalous summer radiation warms the North American continent (Fig. 6a), lowering the surface pressure over land and increasing the surface pressure over the subtropical ocean (Fig. 6c). The intensified Atlantic subtropical high therefore enhances the moisture transport toward, and, in turn, the monsoon rainfall over, the northernmost part of South America, central America, and the North American Southwest (Figs. 6c,b). This direct radiation effect is amplified by a positive oceanic feedback (Fig. 7b). The positive oceanic feedback is associated with a cold equator/warm midlatitude SST anomaly in the eastern tropical North Pacific (Fig. 8g), which enhances the southwesterly wind toward, and, in turn, the precipitation over, the region of North American monsoon. In addition to insolation forcing and wind–evaporation feedback, the northward SST gradient is enhanced by the strong and narrow equatorial cooling in the eastern Pacific (Fig. 8g), which appears to be forced by a stronger easterly trade wind (Fig. 7c) induced by a stronger Asia monsoon (Liu et al. 2000) and ocean–atmospheric feedbacks in the tropical Pacific (Clement et al. 2000).

c. Southern Hemisphere monsoons

The direct effect of the reduced insolation in austral summer is a significant reduction of monsoon precipitation across the SH (Fig. 6e). The oceanic feedback tends to further reduce the monsoon rainfall somewhat in central South America and to increase the monsoon rainfall modestly in South Africa (Fig. 7e). In both cases, the ocean to the west of the continent is warmed with a larger SST anomaly toward high-latitude SH (Fig. 8h). The warmer SSTs induce divergent offshore winds (between 10° and 20°S; Fig. 7f), reducing divergence and, in turn, precipitation over both continents (between 5° and 20°S; Fig. 7e). In eastern Africa south of the

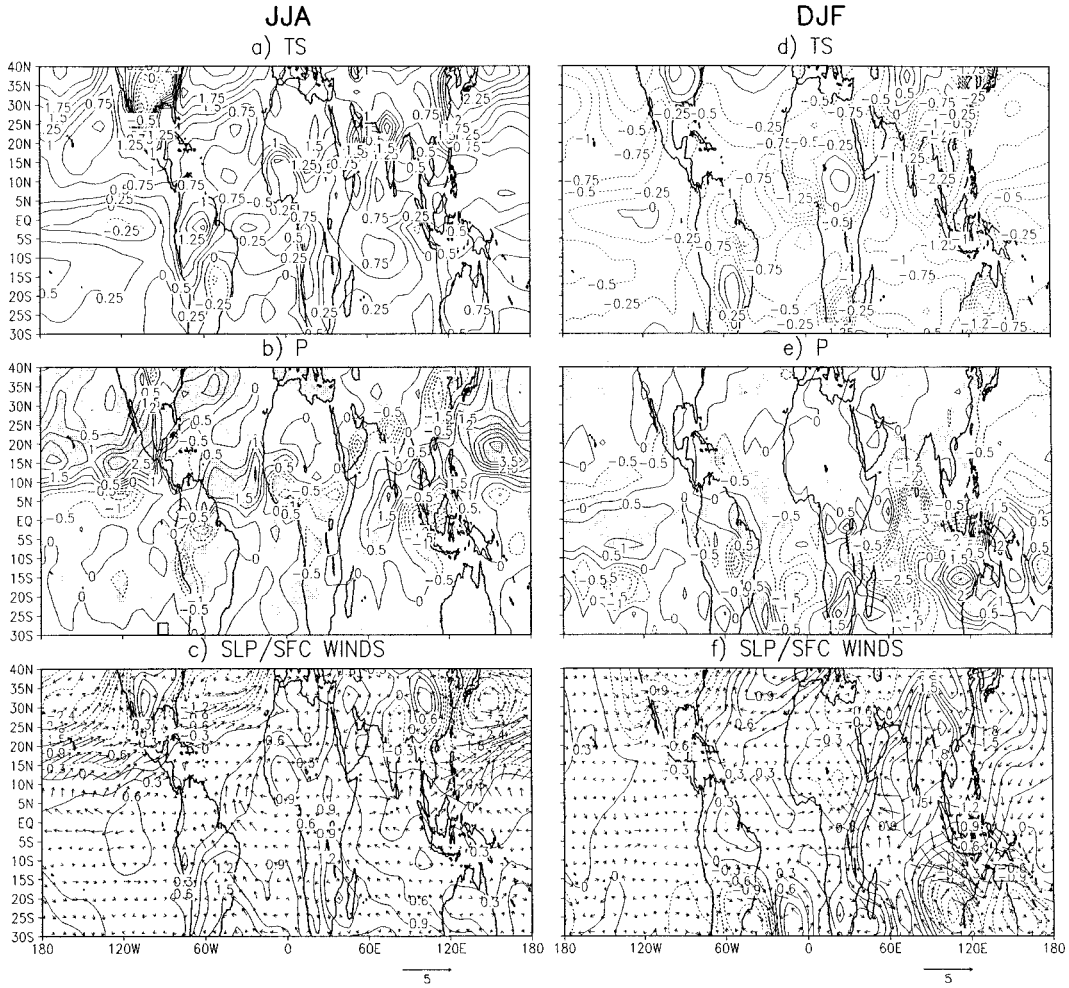

FIG. 7. Oceanic feedback on climate at 11 kyr as simulated from F11k − F11kFix. Plots and units are the same as in Fig. 3. Areas with statistical significance higher than 95% are shaded for the precipitation.

equator, however, a significant onshore wind develops (Fig. 7f), which in turn is forced by a high pressure center to the east (Fig. 7f), stronger upwelling cooling over the eastern North Indian Ocean (Fig. 8h), and eventually stronger Asian winter monsoon. The rainfall increase is larger than the precipitation reduction to the south, resulting in a net oceanic feedback that increases rainfall over the broad region of the South African monsoon. The final change is a reduction of monsoon rainfall, significant in South America but modest in South Africa (Fig. 3e).

In contrast to the reduction of these two SH monsoons (Fig. 3e), the Australian monsoon is enhanced over a significant part of the region because of a dramatic positive feedback from the ocean (Fig. 7e). The overwhelming enhancement of the Australian monsoon by SST changes is accompanied by increased northwesterly surface winds that converge toward northwestern Australia (Fig. 7f). It is important to point out that this increased northwesterly flow is caused not only by the intensification of the NH Asian winter monsoon (Fig. 3f), but also by local ocean dynamics and ocean–atmosphere interaction. The direct NH winter insolation cools surface temperature (Fig. 6d) and increases surface pressure (Fig. 6f) over the Asian continent, strengthening the northerly winter monsoon winds from the Asian continent toward the SH (Fig. 6f; Chang et al. 1979; Lau 1982). If, however, the SST remains unchanged, this remotely forced cross-equatorial wind converges toward (Fig. 6f), and, in turn, causes precipitation over (Fig. 6e), the South Indian Ocean (as opposed to Australia). This occurs because the reduced SH summer insolation establishes an anomalously eastward pressure gradient by increasing the pressure over Australia and lowering pressure over the South Indian Ocean (Fig. 6f). This result is similar to previous AGCM experiments (e.g., Kutzbach and Guetter 1986) and in experiments with an AGCM coupled with a slab ocean (Kutzbach et al. 1998). Therefore, the remote Asian winter monsoon forcing alone, as in previous experiments with AGCMs and coupled AGCM–slab ocean models, is insufficient to enhance the Australian mon-

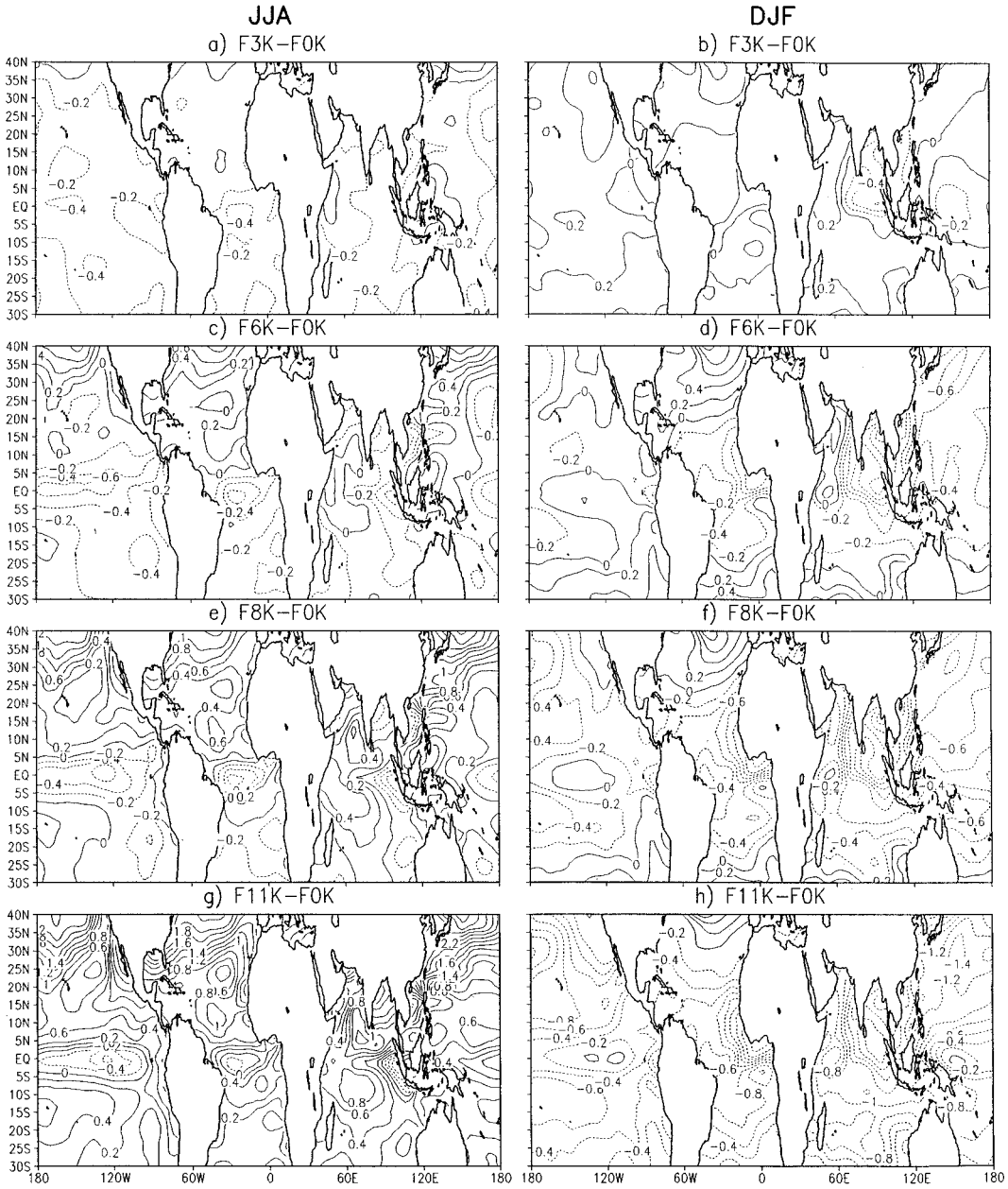

FIG. 8. Seasonal SST anomalies from the present as simulated in coupled FOAM experiments at 3 kyr for (a) JJA and (b) DJF; at 6 kyr for (c) JJA and (d) DJF; at 8 kyr for (e) JJA and (f) DJF; and at 11 kyr for (g) JJA and (h) DJF. Contour interval is 0.2°C.

soon. Instead, local oceanic dynamic response is also necessary.

The reduced pressure over the South Indian Ocean weakens the subtropical high there (Fig. 6f). With a dynamic ocean, the weaker subtropical high reduces the coastal southerly wind and coastal upwelling, generating a warm tongue (warmer relative to the interior South Indian Ocean) along the northwest coast of Australia (Fig. 8h). The warm tongue lowers the surface pressure (relative to interior South Indian Ocean) and establishes a pressure gradient that encourages the cross-equatorial monsoon wind (Fig. 7f) toward, and, in turn, the rainfall (Fig. 7e) over, northwestern Australia. This onshore wind is also enhanced by a stronger upwelling cooling (Fig. 8h) and the associated southerly wind that develops in the North Indian Ocean.

In short, at 11 kyr, the direct insolation forcing tends to increase monsoon in the NH and reduce monsoon in the SH. More complex is the oceanic feedback: it enhances the monsoon significantly in North Africa and modestly in North America, but weakens the monsoon modestly in Asia; it also reduces the monsoon modestly

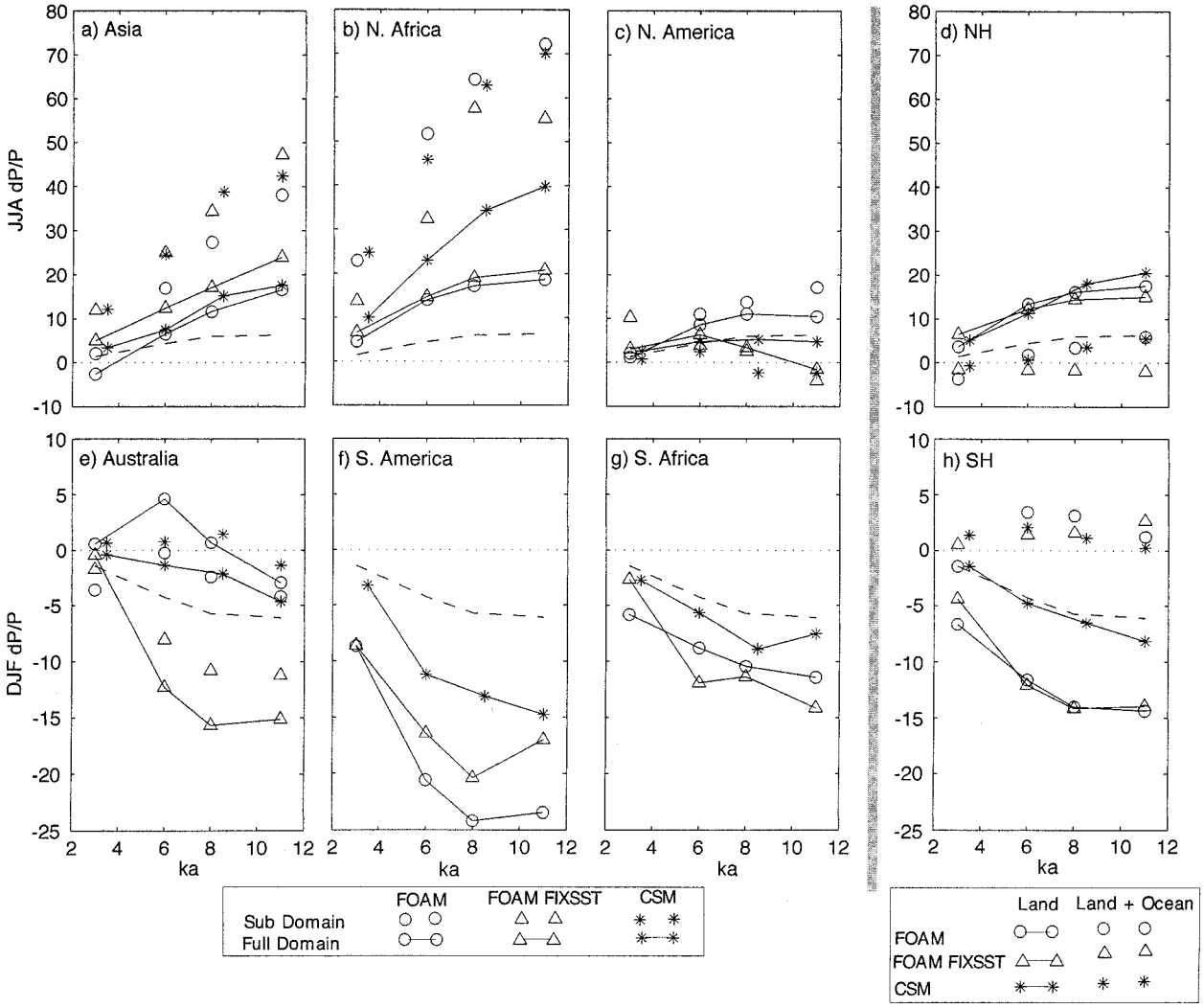

FIG. 9. Relative changes of summer land precipitation anomalies at different times in the Holocene (*x* axis) for the (a) Asian monsoon, (b) North African monsoon, (c) North American monsoon, (d) NH (0°–40°N) in boreal summer (JJA); and (e) Australian monsoon, (f) South American monsoon, (g) South African monsoon, (h) SH (20°S–0°) in austral summer (DJF). The *x* axis is time (in kyr) and the *y* axis is, in percent, the anomaly divided by the 0-kyr mean (multiplied by 100). Circles show the results from the coupled FOAM experiments. Triangles show the results from the fixed SST FOAM AGCM experiments. For reference, the relative change of insolation is also plotted (dashes) for the NH (0°–30°N) summer (JJA) in (a)–(d), and the SH (30°S–0°) summer (DJF) in (e)–(h). For each regional monsoon (a)–(c) and (e)–(f), markers connected by lines are averaged in the large domain (the same as in Fig. 4, except for Australia being 30°S–0°, 110°–150°E), while markers without line connections are for subdomains of 10°–40°N, 60°–100°E in (a), 12°–30°N, 20°W–30°E in (b), 20°–40°N, 110°–60°W in (c), and 20°S–0°, 110°–150°E in (d). In (d) and (h) markers connected by lines are for precipitation over land, while markers without line connections are for both land and ocean (dominated by ocean). Similar to the coupled FOAM experiments, the coupled CSM experiments are shown in asterisks.

in South America, increases the monsoon modestly in South Africa, and increases the monsoon overwhelmingly over northwestern Australia. These responses and oceanic feedbacks are consistent at other Holocene times, as seen in other panels in Figs. 6–8 and the following discussion on Fig. 9.

5. Synthesis of model simulations

We now synthesize the evolution of the six regional monsoons by examining the relative changes of the regionally averaged summer precipitation at succeeding Holocene times (Fig. 9, circles for FOAM and triangles for the fixed SST FOAM).

The summer rainfall over the full domain of the North African monsoon (5°–30°N, 20°W–30°E, markers connected with lines, Fig. 9b) decreases monotonically from the early to the late Holocene by about 20% in FOAM. The precipitation change in this region is dominated by that near the equator in the ITCZ (Fig. 1b). The climate change in the North African semidesert region is better shown by the inland subdomain (12°–30°N, 20°W–30°E;

markers without connection, Fig. 9b). From present to the early Holocene, the relative change of summer rainfall in the northern subdomain increases dramatically by about 60%–80% (due mainly to the smaller mean precipitation), implying a great climate sensitivity there. The effect of oceanic feedback can be quantified by comparing the fixed SST simulations with the coupled simulations. Summer precipitation in the fixed SST simulations also decreases toward the late Holocene (triangles): it reaches only about a half to two-thirds of the precipitation in the coupled FOAM in the inland subdomain but is almost comparable with the coupled FOAM in the full domain. This is consistent with our discussion on Fig. 7b: the oceanic feedback contributes predominantly to the northward expansion, rather than an overall rainfall increase, of the North African monsoon.

Asian monsoon precipitation decreases from the early to late Holocene (Fig. 9a) monotonically in both the full domain (10°–40°N, 60°–120°E) and inland subdomain (consisting of northern India and central western China in 20°–40°N, 60°–100°E). The relative changes of the monsoon rainfall in both the full and inland subdomains are about half that in North Africa, suggesting a much higher monsoon sensitivity to the orbital forcing in North Africa than in Asia. Both monsoon changes, however, are amplified relative to the local summer insolation (dashes), the latter decreasing by only about 7% through the Holocene. A major difference from the North African monsoon is the negative oceanic feedback on the Asian monsoon. This negative feedback can be seen from the greater monsoon precipitation in the fixed SST simulations (triangles, Fig. 9a) compared to the respective coupled simulations (circles) in both the full and subdomains. Furthermore, the oceanic feedback reduces the precipitation significantly over the full Asian domain (about one-third to a half), but less significantly in the inland northwestern subdomain (Fig. 9a). This is consistent with Fig. 7b: the oceanic feedback reduces summer rainfall over the Asian monsoon region, mainly in eastern China.

Summer precipitation also decreases toward the late Holocene in the full domain of North and Central America and northernmost South America (0°–40°N, 110°–60°W; Fig. 9c). In contrast to the canonical response, however, the ocean excerts a positive feedback on monsoon precipitation (Fig. 9c). The relative change of monsoon rainfall, however, is only about 10%, comparable with the change of summer insolation and much less than for the other two NH monsoons. It should be recognized, however, that the precipitation averaged over the full domain reflects mainly the tropical rainfall in Central America and the northernmost part of South America. In the subdomain of North America (20°–40°N, 110°–90°W), summer precipitation appears to increase.

In the SH, the direct insolation forcing would have reduced monsoon precipitation by only about 15% in the early and mid-Holocene in all three monsoon regions (triangles, Figs. 9e–g). This drying is intensified slightly by the oceanic feedback over South America (Fig. 9f), but is reduced modestly in South Africa (Fig. 9g), due to modest oceanic feedback (Figs. 7e,f). The insolation-induced drying is completely reversed over the full domain of the Australian monsoon (30°S–0°, 110°–150°E) by an overwhelming oceanic feedback that eventually increases the total monsoon rainfall slightly in the Holocene (Fig. 9e). In the subdomain of northwestern Australia (20°S–0°, 110°–150°E), the total monsoon precipitation is virtually unchanged in FOAM, because the reduction of Australian monsoon precipitation due to local radiation is largely canceled by the oceanic feedback there.

Finally, summer rainfall over the entire tropical lands of the NH (0°–40°N) and the SH (20°S–0°) are plotted in Figs. 9d and 9h, respectively. Total land precipitation increases by about 20% in the early Holocene in the NH, about two to three times that of the summer insolation increase, and decreases less than 15% in the SH. Furthermore, oceanic feedback is not significant when averaged over all the land, due to the cancellation of positive and negative feedbacks in different regions. Averaged over the entire ocean and land area, precipitation increases in the NH by less than 10% due to the dominance of land precipitation increase and increases slightly in the SH due to the dominant hemispheric influence from the ocean there.

Finally, we note that the relative change of the annual mean precipitation is largely similar to the summer change in Fig. 9 for each monsoon (especially in the NH), but with a smaller magnitude (not shown).

6. Comparison with paleoclimate records

A detailed comparison of the model simulations and updated observations at 6 kyr will be reported in Harrison et al. (2003) for the North American monsoon, and in L02 for the global monsoons. Here, we only compare some major features of our simulations with published observations for the Holocene and show that they are in overall good agreement.

The simulated decrease of the North African monsoon and Asian monsoon from the early Holocene toward the present is consistent with the generally decreasing wetter conditions in North Africa and most of southern and eastern Asia (Kutzbach and Street-Perrott 1985). Pollen records and lake status show much wetter conditions in North Africa in the early Holocene (Street-Perrott and Perrott 1993; Kohfeld and Harrison 2000) and a northward expansion of 10° latitude of moisture-demanding vegetation (Joussaume et al. 1999). Lake status records and other paleoclimate records in the Asian monsoon region also show increased monsoon activity in the early Holocene, then decreasing to the present (Winkler and Wang 1993; Kohfeld and Harrison 2000; Yu et al. 1998, 2001). The stronger sensitivity of the North African

monsoon, compared to the Asian monsoon, is also consistent with paleoclimate records. The North African monsoon is observed to have collapsed rapidly within several centuries after the mid-Holocene (deMenocal et al. 2000), while there is no record of such dramatic changes of the Asian monsoon in the late Holocene. Our model still underestimates the abruptness and extent of the northward expansion of the North African monsoon, due perhaps to the lack of additional feedback processes such as the vegetation feedback (Kutzbach et al. 1996; Claussen et al. 1999; Doherty et al. 2000). The simulated monsoon enhancement in the American Southwest and the drier conditions in the surrounding region are also in good agreement with observations. One should refer to Harrison et al. (2003) for a more detailed data–model comparison.

The dry conditions simulated in South America are in broad agreement with paleoclimate observations. Dry conditions in the early to mid-Holocene are consistent with the low lake levels in Peruvian Lake Junin (Seltzer et al. 2000) and Lake Titicaca (Wirrman and Mourguiart 1995). The model results are also consistent with the pollen records from the southern margin of Amazonian rain forest, which show that the humid evergreen rainforest of eastern Bolivia expanded southward over the past 3000 years and that the present-day limit represents the southernmost extent of the Amazonian rain forest over at least the past 50 000 years (Mayle et al. 2000). The snow accumulation on Sajama Mountain also has increased from the early Holocene toward the present (Thompson et al. 1998). Finally, and perhaps most comprehensively, oxygen isotopic composition of planktonic foraminifera recovered from a marine sediment core in the region of Amazon River discharge suggests that the Amazon River discharge was reduced significantly (up to 50%) in the early Holocene and gradually recovered toward the present (Maslin and Burns 2000).

Very limited data are published on the South African monsoon. There appears to be no strong drying evidence in the southern Africa region. Indeed, some paleodata, such as lake level, show a slightly wetter condition over parts of southern Africa (Street-Perrott and Perrott 1993). This appears to agree with our simulation in the sense that the simulated drying is less pronounced in South Africa than in South America.

The simulated enhancement of the Australian monsoon agrees with observations. Paleohydrological studies of ancient foreshore dunes suggest the presence of cycles of megalakes in northwestern Australia in the late quaternary (Bowler et al. 2001). Proxy evidence has suggested limited Australian monsoon activity during the last glacial maximum (LGM) and modest reinvigoration in the Holocene (Markgraf et al. 1992). The carbon isotopes in fossil emu eggshells from Lake Eyre, southern Australia, suggest substantial variation of the relative abundance of C_4 grasses in the last 65 ka. This study implies a recovery of the Australian monsoon from a dry period in the LGM toward the early to mid-Holocene (Johnson et al. 1999). A paleohydrological study of the drainage basins in the Kimberley region of monsoonal northwestern Australia suggests that the Australian monsoon became active as early as 14 kyr (Wyrwoll and Miller 2001). A study of the thermoluminescence ages of plunge-pool sediments near Darwin, Australia (Nott and Price 1994), and evidence from alluvial sedimentation along the Gilbert River, Gulf of Carpentaria (Nanson et al. 1991), also imply a more intense monsoon in the early Holocene rather than after 5 kyr. This Australian monsoon activity, at odds with the direct insolation forcing, has not been explained in the past. Here, our coupled model suggests that local oceanic feedback may have played a critical role in activating the Australian monsoon in the early Holocene.

Finally, oceanic observations are much less complete than terrestrial observations in the Holocene and need to be improved significantly to allow for a meaningful model–data comparison. Nevertheless, some preliminary comparisons of available data, although tentative, can be made in the Holocene (Liu et al. 2003). Regarding the oceanic feedback on monsoon, the SSTs in the early and mid-Holocene tend to be colder than today in the equatorial Atlantic, but warmer than today in the western subtropical North Atlantic (Ruddiman and Mix 1993). This is consistent with our Holocene SSTs (Fig. 8) and may provide indirect support for the positive oceanic feedback on the North African monsoon. In the tropical Pacific, recent observations suggest a western Pacific warm pool SST warmer in summer and colder in winter in the early Holocene, decreasing toward the mid-Holocene (Stott et al. 2002), consistent with our model results (Fig. 8) and our SST feedback on the Asian monsoon. In the eastern equatorial Pacific cold tongue, SSTs are reduced compared with the present, especially in the mid-Holocene (Koutavas et al. 2002), consistent with our simulation qualitatively (Fig. 8) and our SST feedback on North American monsoon. In the SH, the reconstructed SST shows a warming along the southwestern coasts of Africa and South America (Morley and Dworetzky 1993). This is consistent with our model simulations (Fig. 8). Since these west coast warming tongues are generated similar to that near the northwestern Australia, these observations may provide indirect support for the positive oceanic feedback on the Australian monsoon.

7. Summary and discussion

The evolution of six major summer monsoons is studied in FOAM under the insolation forcing at 11, 8, 6, and 3 kyr. It is found that the monsoon responses differ substantially among different regions, partly due to very different oceanic feedbacks. In the NH, all the simulated monsoons show a significant enhancement in the early Holocene and a reduction toward the present. The enhanced summer insolation provides the major forcing

for the observed monsoon intensification, especially in the early Holocene. Oceanic feedback further enhances the monsoon significantly in North Africa and modestly in North America, but weakens the monsoon in South Asia–East Asia. In the SH, the South American monsoon and, to some extent, the South African monsoon are weakened, mainly by the reduction of the local summer insolation. However, the Australian monsoon is enhanced modestly because of an overwhelming oceanic positive feedback there.

The North African monsoon, especially in northern inland Africa, shows the strongest sensitivity to the orbital forcing, due to the combination of the insolation forcing and positive oceanic feedback. Relatively, the sensitivity of the Asian monsoon is smaller, partly because of a negative oceanic feedback. Relative to the change of summer insolation (up to 7% at 11 kyr), the change of monsoon precipitation is more than three times larger in the North African and Asian monsoons but has a comparable magnitude in other regions. In Australia, even the sign of the monsoon change is opposite to the local radiation change.

Our coupled FOAM (F0k − F11k) simulations are in overall agreement with a similar set of simulations in the NCAR CSM (see appendix), suggesting that our major conclusions on the evolution of the Holocene monsoon are robust in both models. The mechanisms associated with oceanic feedback, however, cannot be directly verified with the CSM because of the lack of parallel fixed SST experiments in CSM.

Oceanic feedbacks differ dramatically from that in the canonical monsoon response. The positive oceanic feedback in North Africa is perhaps the most robust and has been reproduced in all coupled models so far (Kutzbach and Liu 1997; Hewitt and Mitchell 1998; Liu et al. 1999; Braconnot et al. 2000). In the region of the North American monsoon, a somewhat similar positive oceanic feedback is present in FOAM (Harrison et al. 2003), but it has not been carefully analyzed in other studies. These SST–monsoon rainfall relationships are consistent with those for present interannual variability [e.g., Hastenrath (1978) for North Africa, and Higgins and Shi (2000) for the North America], further supporting the physical consistency of the oceanic feedback in the Holocene. In the SH, the ocean exerts an overwhelming positive feedback on the Australian monsoon, but only modest feedback to the South African and South American monsoons.

The nature of the SST feedback seems to be most uncertain in the Asian monsoon region. Our FOAM study finds a negative oceanic feedback, which is consistent with a previous study with an asynchronously coupled model (Liu et al. 1999), but disagrees with two recent coupled ocean–atmosphere simulations (Hewitt and Mitchell 1998; Braconnot et al. 2000), both of which seem to suggest an enhancement of Asian monsoon by oceanic feedback. This inconsistency between models is perhaps not surprising, since the Asian monsoon, which consists of the two independent South Asia and East Asia regional monsoons, has complex dynamics and involves processes in the Tropics as well as in the extratropics (Lau et al. 2000). Our study of the oceanic feedback on the Asian monsoon, in some sense, resembles present studies of the monsoon–ENSO relationship. In spite of the recognition of the significant influence of the Indo-Pacific SST on the Asian monsoon (Shukla 1987; Webster et al. 1998; Wang et al. 2001; Lau and Wu 2001), the specific process for the SST to affect the monsoon remains not fully understood. On the one hand, a La Niña–like SST in boreal summer, as in the early to mid-Holocene (Figs. 8a,c,e,g), should help to establish deep convection over the western Pacific and Indian Oceans, favoring the enhanced southern Asian monsoon, as reflected in the present-day negative correlation of the eastern Pacific SST and Indian rainfall (Shukla 1987; Webster et al. 1998). On the other hand, a cold equatorial SST induces an anomalous low pressure over the western tropical North Pacific due to forced equatorial Rossby waves. The cyclonic circulation can feed back positively with the local SST, through the wind–evaporation feedback, and therefore enhance the warm SST anomaly in the tropical western North Pacific. The increased warm SST further enhances the cyclonic circulation, whose southward wind over East Asia suppresses the monsoon moisture transport and, in turn, the East Asia monsoon rainfall (Wang et al. 2000). Therefore, the final impact of SST on the Asian monsoon could be sensitive to the competition of opposing mechanisms.

In addition to the orbital forcing and oceanic feedback, it has become clear that land surface feedback has important impacts on regional climates, notably over North Africa (Texier et al. 1997; Broström et al. 1998; Braconnot et al. 1999; Doherty et al. 2000). The role of the three major climate forcing processes (radiation, ocean feedback, and land feedback) may differ from region to region and therefore need to be assessed with further modeling studies in fully coupled ocean–atmosphere–land vegetation models. Comparisons are also needed between various coupled climate models to identify the robust climate response. Finally, paleoclimate observations need to be improved, especially over the ocean, to allow for a complete model–data comparison of the evolution of each monsoon in the Holocene.

Acknowledgments. We would like to thank Drs. S. Hastenrath, A. Hammer, J. Betancourt, S. Harrison, and K.-H. Wyrwoll for helpful discussions and useful references. We thank Dr. L. Wu for performing all the FOAM experiments. ZL thanks NCAR for their hospitality during his sabbatical stay there. This paper is a contribution to the Testing Earthsystem Models with Palaeoenvironmental Observations (TEMPO) project. The work is supported by ESH/Paleoclimate Program of NSF. The computations are performed at the Supercomputing Center at NCAR.

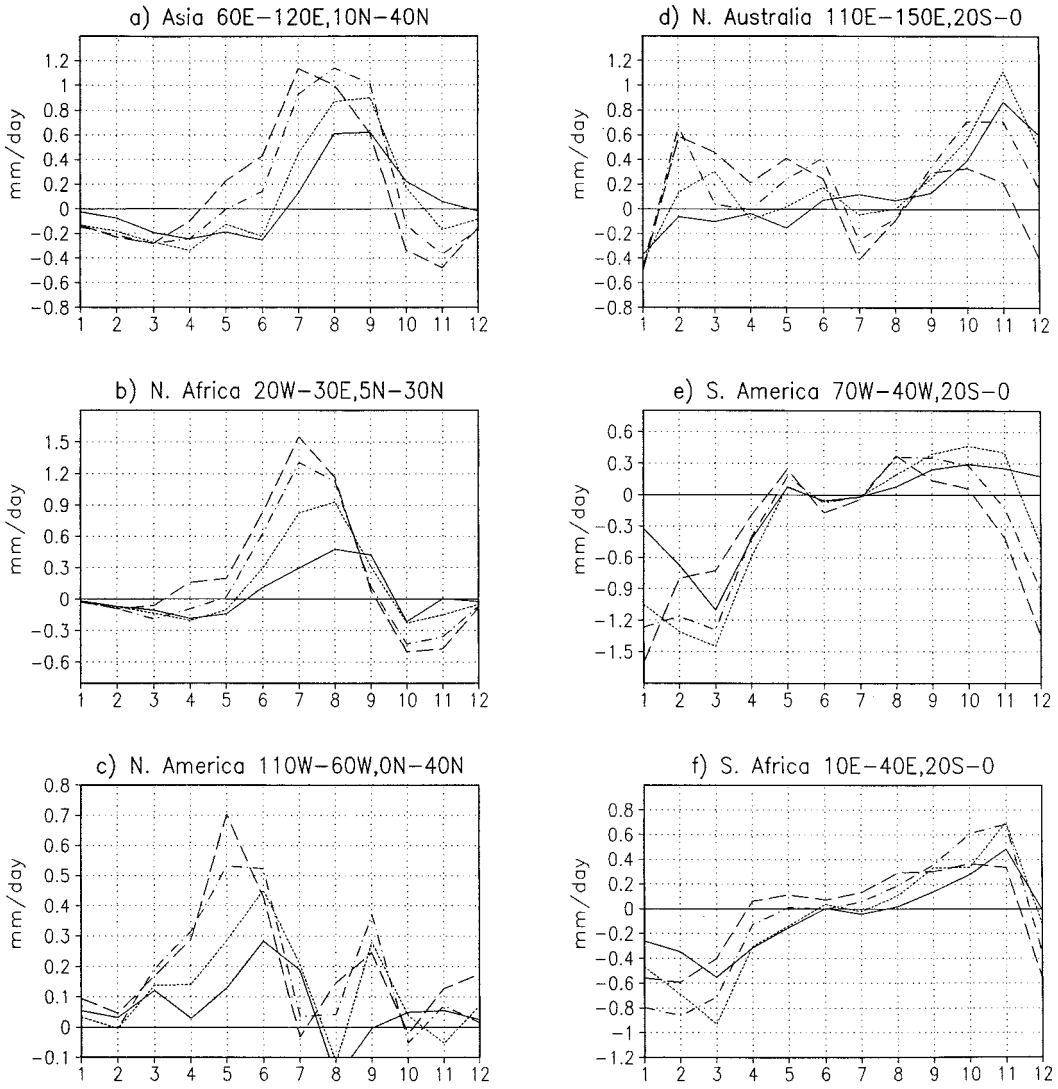

FIG. A1. The same as in Fig. 4, but for the monthly evolution of precipitation anomalies from the present at 3.5, 6, 8.5, and 11 kyr in CSM.

APPENDIX

Holocene Monsoon Simulation in NCAR CSM

The NCAR CSM is a fully coupled climate model, consisting of an AGCM, an OGCM, a dynamic sea ice model, and a land surface biophysics model (Boville and Gent 1998). The version of the CSM that we used has a resolution of T31 (equivalent grid spacing about 3.75° × 3.75°) for the atmosphere and land surface components, and a variable three-dimensional grid (25 vertical levels, 3.6° longitude grid spacing, and a latitude spacing of 1.8° poleward of 30°, decreasing to 0.9° within 10° of the equator) for the ocean and sea ice models (Otto-Bliesner and Brady 2001).

Four CSM experiments—C3.5k, C6k, C8.5k, and C11k—are forced the same as the control run (C0k) except that the insolation forcing is set at 3.5, 6, 8.5, and 11 kyr, respectively. In all the experiments, the CO_2 level is kept at the preindustrial level of 280 ppmv. All of the CSM experiments are integrated for 100 yr with the last 50 yr being averaged for the monthly ensemble. No fixed SST experiments are performed in CSM. Since the slight offset of orbital forcing parameters between the CSM and FOAM at 3 and 3.5 kyr, and 8 and 8.5 kyr produces only a small difference in the forcing relative to the large changes during Holocene (e.g., the insolation difference of 3 to 3.5 kyr is about 15% of that from 3 to 6 kyr, as seen in Fig. 9), the coupled CSM experiments are similar to the coupled FOAM experiments and therefore should provide a valuable model–model comparison. The two models differ in resolution, some physical parameterizations, and different ocean and sea ice models. It is therefore encouraging to find that the two models show an overall consistency

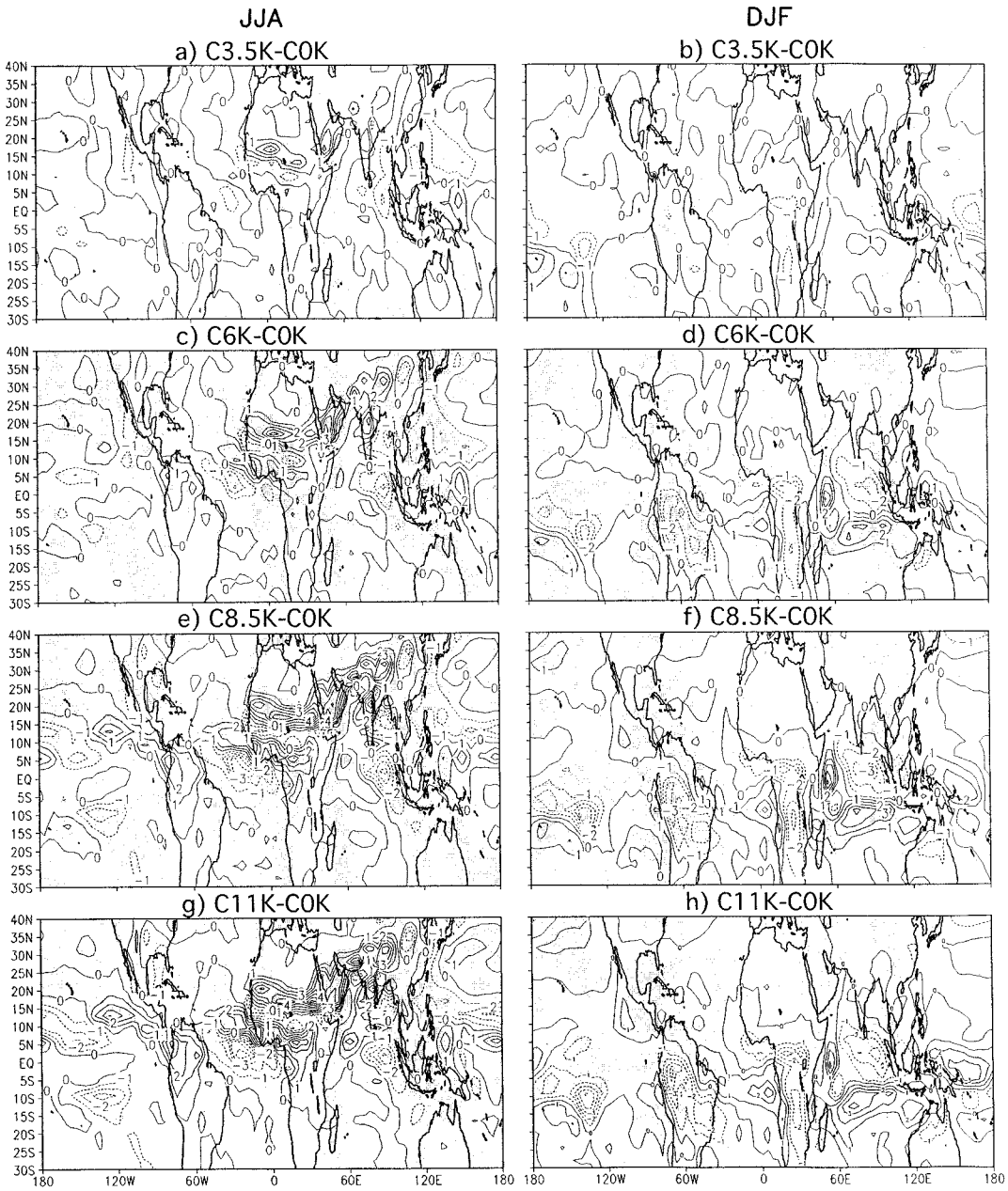

FIG. A2. Patterns of the precipitation anomaly from the present simulated in CSM for boreal summer and winter at (a), (b) 3.5 kyr (C3.5k − C0k), (c), (d) 6 kyr (C6k − C0k), (e), (f) 8.5 kyr (C8.5k − C0k), and (g), (h) 11 kyr (C11k − C0k). The contour interval is 1 mm day^{-1}.

in the major features of the Holocene climate, as described briefly below.

The seasonal cycle and pattern of the precipitation changes from early Holocene to present in CSM are broadly consistent with FOAM. In North Africa, the CSM seasonal precipitation anomaly shows summer rainfall that is strongest in the early Holocene and weakens toward the late Holocene (Fig. A1b) and Asia (Fig. A1a), and the Holocene summer rainfall anomalies are also characterized by a pair of positive and negative zonal bands in North Africa (Figs. A2a,c,e,g). In South Asia–East Asia, the CSM Holocene precipitation anomaly exhibits modest negative anomalies in southwestern India and eastern China, surrounded by strong positive anomalies. Holocene summer precipitation in CSM is increased over the America Southwest and the northernmost part of South America (Figs. A2a,c,e,g). Over South America and South Africa, Holocene CSM precipitation is reduced in austral summer and increased somewhat in late spring (Figs. A1e,f) with dominant

negative precipitation anomaly patterns (Figs. A2b,d,f,h) similar to those in FOAM. Finally, summer monsoon rainfall is enhanced in the northwestern corner of Australia and in Papua New Guinea in the early to mid-Holocene (Figs. A2b,d,f,h).

The similarity of CSM and FOAM can also be seen in the evolution of the regional monsoon rainfall as synthesized in Fig. 9 (asterisks): in the NH, the sensitivity of the monsoon is the strongest in North Africa, modest in Asia, and weak in North America (Figs. 9a–c); in the SH, monsoon reduction is the strongest in South America, modest in South Africa, and unchanged or even increased slightly in northwest Australia (Figs. 9e–g).

There are, as expected, quantitative differences between the simulations of the two models. For example, in contrast to a single peak in August in FOAM (Fig. 4c), the increase of North American monsoon in CSM shows a double peak in May and September (Fig. A1c), which is associated with the rainfalls over central America–northernmost South America and the America Southwest, respectively. This difference may be related to the coarse resolution of the FOAM atmosphere and its representation of the ITCZ near the region. As another example, the penetration of the positive monsoon rainfall anomalies into northwestern Australia is weaker in CSM (Figs. A2d,f,h) than in FOAM (Figs. 5d,f, 3e) in the early to mid-Holocene. As a result, the increase of Australian monsoon is less in CSM (Fig. A1d) than in FOAM (Fig. 4d). The weaker change of Australian monsoon may be related to the zonal ocean resolution in CSM, which may be less efficient to generate coastal upwelling there. A detailed comparison of the results of the two models are beyond the scope of this paper. In spite of some quantitative differences, it is assuring to us that the two models agree with each other qualitatively on most major features of the evolution of global monsoons.

REFERENCES

Adams, D. K., and A. C. Comrie, 1997: The North American monsoon. *Bull. Amer. Meteor. Soc.,* **78,** 2197–2213.

Berger, A. L., 1978: Long-term variations of daily insolation and Quaternary climatic changes. *J. Atmos. Sci.,* **35,** 2362–2367.

Betancourt J. L., 2000: The Amazon reveals its secrets—partly. *Science,* **290,** 2274–2275.

Boville, B. A., and P. Gent, 1998: The NCAR Climate System Model, version one. *J. Climate,* **11,** 1115–1130.

Bowler, J. M., K.-H. Wyrwoll, and Y. Lu, 2001: Variations of the northwest Australian summer monson over the last 300,000 years: The paleohydrological record of the Gregory (Mulan) Lakes system. *Quat. Int.,* **83–85,** 63–80.

Braconnot, P., S. Joussaume, O. Marti, and N. de Noblet, 1999: Synergistic feedbacks from ocean and vegetation on the African monsoon response to mid-Holocene insolation. *Geophys. Res. Lett.,* **26,** 2481–2484.

——, O. Marti, S. Joussaume, and Y. Leclainche, 2000: Ocean feedback in response to 6ka BP insolation. *J. Climate,* **13,** 1537–1553.

Broström, A., M. Coe, S. P. Harrison, R. Gallimore, J. E. Kutzbach, J. Foley, I. C. Prentice, and P. Behling, 1998: Land surface feedbacks and palaeomonsoons in Northern Africa. *Geophys. Res. Lett.,* **25,** 3615–3618.

Chang, C. P., J. E. Erickson, and K. M. Lau, 1979: Northeasterly cold surges and near-equatorial disturbances over the winter MONEX area during December 1974. Part I: Synoptic aspects. *Mon. Wea. Rev.,* **107,** 812–824.

Claussen, M., C. Kubatzki, V. Bovkin, A. Ganopolski, P. Hoelzmann, and H.-J. Pachur, 1999: Simulation of an abrupt change in Saharan vegetation in the mid-Holocene. *Geophys. Res. Lett.,* **26,** 2037–2040.

Clement, A. C., R. Seager, and M. Cane, 2000: Suppression of El Nino during the mid-Holocene by changes in the Earth's orbit. *Paleoceanography,* **15,** 731–741.

COHMAP Members, 1988: Climatic changes of the past 18,000 years: Observations and model simulations. *Science,* **241,** 1043–1052.

deMenocal, P., J. Ortiz, T. Guilderson, J. Adkins, M. Sarnthein, L. Baker, and M. Yarusinsky, 2000: Abrupt onset and termination of the African humid period: Rapid climate response to gradual insolation forcing. *Quat. Sci. Rev.,* **19,** 347–361.

Doherty, R., J. E. Kutzbach, J. Foley, and D. Pollard, 2000: Fully coupled climate/dynamical vegetation model simulations over Northern Africa during the mid-Holocene. *Climate Dyn.,* **16,** 561–573.

Douglas, M. W., R. A. Maddox, K. Howard, and S. Reyes, 1993: The Mexican monsoon. *J. Climate,* **6,** 1665–1677.

Harrison, S. P., and J. Dodson, 1993: Climates of Australia and New Guinea since 18,000 yr BP. *Global Climates since the Last Glacial Maximum,* H. E. Wright et al., Eds., University of Minnesota Press, 265–293.

——, J. E. Kutzbach, Z. Liu, P. J. Bartlein, D. Mubs, I. C. Prentice, and R. Thompson, 2003: Mid-Holocene climates of the Americas: A dynamical response to changed seasonality. *Climate Dyn.,* **20,** 663–688.

Hastenrath, S., 1978: On modes of tropical circulation and climate anomalies. *J. Atmos. Sci.,* **35,** 2222–2231.

——, 1994: *Climate Dynamics of the Tropics*. Kluwer Academic, 488 pp.

Hewitt, C. D., and J. F. B. Mitchell, 1998: A fully-coupled GCM simulation of the climate of the mid-Holocene. *Geophys. Res. Lett.,* **25,** 361–364.

Higgins, R. W., and W. Shi, 2000: Dominant factors responsible for interannual variability of the summer monsoon in the southwestern United States. *J. Climate,* **13,** 759–776.

——, Y. Yao, and X. L. Wang, 1997: Influence of the North American monsoon system on the U.S. summer precipitation regime. *J. Climate,* **10,** 2600–2622.

Jacob, R., 1997: Low frequency variability in a simulated atmosphere ocean system. Ph.D. thesis, University of Wisconsin—Madison, 177 pp.

Johnson, B. J., G. H. Miller, M. L. Fogel, J. W. Magee, M. K. Gagan, and A. R. Chivas, 1999: 65,000 years of vegetation change in central Australia and the Australian summer monsoon. *Science,* **284,** 1150–1153.

Joussaume S., and PMIP members, 1999: Monsoon changes for 6000 years ago: Results of 18 simulations from the Paleoclimate Modeling Intercomparison Project (PMIP). *Geophys. Res. Lett.,* **26,** 859–862.

Kohfeld, K. E., and S. P. Harrison, 2000: How well can we simulate past climates? Evaluating the models using global palaeoenvironmental data sets. *Quat. Sci. Rev.,* **19,** 321–346.

Koutavas, A., J. Lynch-Stieglitz, T. M. Marchitto Jr., and J. P. Sachs, 2002: El Nino-like patterns in ice age tropical Pacific sea surface temperature. *Science,* **297,** 226–230.

Kutzbach, J. E., and B. I. Otto-Bliesner, 1982: The sensitivity of the African–Asian monsoonal climate to orbital parameter changes for 9000 yr B. P. in a low-resolution general circulation model. *J. Atmos. Sci.,* **39,** 1177–1188.

——, and F. A. Street-Perrott, 1985: Milankovitch forcing of fluctuations in the level f tropical lakes from 18 to 0kyr BP. *Nature,* **317,** 130–140.

——, and P. Guetter, 1986: The influence of changing orbital param-

eters and surface boundary conditions on climate simulations for the past 18 000 years. *J. Atmos. Sci.,* **43,** 1726–1759.
——, and R. G. Gallimore, 1988: Sensitivity of a coupled atmosphere/mixed layer ocean model to changes in orbital forcing at 9000 years B. P. *J. Geophys. Res.,* **93,** 803–821.
——, and T. Webb III, 1993: Conceptual basis for understanding late-Quaternary climates. *Global Climates since the Last Glacial Maximum,* H. E. Wright et al., Eds., University of Minnesota Press, 5–11.
——, and Z. Liu, 1997: Oceanic feedback on the western African monsoon at 6000 BP. *Science,* **278,** 440–443.
——, G. Bonan, J. Foley, and S. P. Harrison, 1996: Vegetation and soil feedbacks on the response of the African monsoon to orbital forcing in the early to middle Holocene. *Nature,* **384,** 623–626.
——, R. Gallimore, S. Harrison, P. Behling, R. Selin, and F. Larrif, 1998: Climate and biome simulations for the past 21,000 years. *Quat. Sci. Rev.,* **17,** 473–506.
Lau, K.-M., 1982: Equatorial response to northeasterly cold surges during winter monsoon as inferred from satellite cloud imageries. *Mon. Wea. Rev.,* **110,** 1306–1313.
——, and H. T. Wu, 2001: Intrinsic coupled ocean–atmosphere modes of the Asian summer monsoon: A reassessment of monsoon–ENSO relationships. *J. Climate,* **14,** 2880–2895.
——, K.-M. Kim, and S. Yang, 2000: Dynamical and boundary forcing characteristics of regional components of the Asian summer monsoon. *J. Climate,* **13,** 2461–2482.
Liu, Z., R. Gallimore, J. Kutzbach, W. Xu, Y. Golubev, P. Behling, and R. Siegle, 1999: Modeling long term climate change with the Equilibrium Asynchronous Coupling scheme. *Climate Dyn.,* **15,** 325–340.
——, J. Kutzbach, and L. Wu, 2000: Modeling climate shift of El Nino variability in the Holocene. *Geophys. Res. Lett.,* **27,** 2265–2268.
——, E. Brady, and J. Lynch-Stieglitz, 2003: Global ocean response to orbital forcing in the Holocene. *Paleoceanography,* in press.
Markgraf, V., 1993: Climatic history of central and south America since 18,000 yr B.P.: Comparison of pollen records and model simulation. *Global Climates since the Last Glacial Maximum,* H. E. Wright et al., Eds., University of Minnesota Press, 357–385.
——, J. R. Dodson, A. P. Kershaw, M. S. McGloe, and N. Nicholls, 1992: Evolution of late Pleistocene and Holocene climates in the circum-South Pacific land areas. *Climate Dyn.,* **6,** 193–211.
——, and Coauthors, 2000: Paleoclimate reconstruction along the Pole–Equator–Pole transect of the Americas (PEP 1). *Quat. Sci. Rev.,* **19,** 125–140.
Maslin, M. A., and S. J. Burns 2000: Reconstruction of the Amazon basin effective moisture available over the past 14,000 years. *Science,* **290,** 2285–2287.
Mayle, F. E., R. Burbridge, and T. J. Killen, 2000: Millennial-scale dynamics of southern Amazonian rain forest. *Science,* **290,** 2291–2294.
Metcalfe, S. E., S. L. O'Hara, M. Caballero, and S. J. Davies, 2000: Records of late Pleistocene–Holocene climatic change in Mexico—A review. *Quat. Sci. Rev.,* **19,** 699–721.
Mitchell, J. F. B., N. S. Grahame, and K. J. Needam, 1988: Climate simulation for 9000 years before present: Seasonal variations and effect of the Laurentide Ice Sheet. *J. Geophys. Res.,* **93** (D7), 8283–8303.
Morley, J. J., and B. A. Dworetzky, 1993: Holocene temperature patterns in the South Atlantic, Southern, and Pacific Oceans. *Global Climates since the Last Glacial Maximum,* H. E. Wright et al., Eds., University of Minnesota Press, 125–135.
Nanson, G. C., D. M. Price, S. A. Short, R. W. Young, and B. G. Jones, 1991: Comparative uranium–thorium dating and thermoluminescence dating of weathered Quaternary alluvium in the tropics of northern Australia. *Quat. Res.,* **35,** 347–366.
Nott, J., and D. M. Price, 1994: Plunge pools and paleoprecipitation. *Geology,* **22,** 1047–1050.
Otto-Bliesner, B. L., 1999: El Nino/La Nina and Sahel precipitation during the middle Holocene. *Geophys. Res. Lett.,* **26,** 87–89.
——, and E. C. Brady, 2001: Tropical Pacific variability in the NCAR Climate System Model. *J. Climate,* **14,** 3587–3607.
Ruddiman, W. F., and A. C. Mix, 1993: The North and equatorial Atlantic at 9000 and 6000 yr B.P. *Global Climates since the Last Glacial Maximum,* H. E. Wright et al., Eds., University of Minnesota Press, 94–124.
Seltzer, G., D. Rodbell, and S. J. Burns, 2000: Isotopic evidence for Late Glaical and Holocene climatic change in the tropical Andes. *Geology,* **28,** 35–38.
Shukla, J., 1987: Interannual variability of monsoons. *Monsoons,* J. S. Fein and P. L. Stephens, Eds., John Wiley and Sons, 399–464.
Stott, L., C. Poulsen, S. Lund, and R. Thunell, 2002: Super ENSO and global climate oscillations at millennial time scales. *Science,* **297,** 222–226.
Street-Perrott, F. A., and R. A. Perrott, 1993: Holocene vegetation, lake levels and climate of Africa. *Global Climates since the Last Glacial Maximum,* H. E. Wright et al., Eds., University of Minnesota Press, 318–356.
Suppiah, R., 1992: The Australian summer monsoon: A review. *Prog. Phys. Geogr.,* **16,** 283–318.
Tang, M., and E. R. Reiter, 1984: Plateau monsoons of the Northern Hemisphere: A comparison between North America and Tibet. *Mon. Wea. Rev.,* **112,** 617–637.
Texier, D., and Coauthors, 1997: Quantifying the role of biosphere–atmosphere feedbacks in climate change: Coupled model simulation for 6000 years BP and comparison with palaeodata for northern Eurasia and northern Africa. *Climate Dyn.,* **13,** 865–882.
Thompson, L. G., and Coauthors, 1998: A 25,000-year tropical climate history from Bolivian ice cores. *Science,* **282,** 1858–1864.
Thompson, R. S., C. Whitlock, P. J. Bartlein, S. P. Harrison, and W. G. Spaulding, 1993: Climatic changes in the western United States since 18,000 yr B.P. *Global Climates since the Last Glacial Maximum,* H. E. Wright et al., Eds., University of Minnesota Press, 468–513.
Wang, B., R. Wu, and X. Fu, 2000: Pacific–East Asian teleconnection: How does ENSO affect East Asian climate? *J. Climate,* **13,** 1517–1536.
——, ——, and K.-M. Lau, 2001: Interannual variability of the Asian summer monsoon: Contrasts between the Indian and the western North Pacific–East Asian monsoons. *J. Climate,* **14,** 4073–4090.
Webb, T., P. Partlein, S. P. Harrison, and K. H. Anderson, 1993: Vegetation, lake levels, and climate in eastern North America for the past 18,000 years. *Global Climates since the Last Glacial Maximum,* H. E. Wright et al., Eds., University of Minnesota Press, 415–467.
Webster, P. J., V. O. Magana, T. N. Palmer, J. Shukla, R. A. Tomas, M. Yanai, and T. Yasunari, 1998: Monsoons: Processes, predictability, and the prospects for prediction. *J. Geophys. Res.,* **103,** 14 451–14 510.
Winkler, M. G., and P. K. Wang, 1993: The late-Quaternary vegetation and climate of China. *Global Climates since the Last Glacial Maximum,* H. E. Wright et al., Eds., University of Minnesota Press, 221–264.
Wirrman, D., and P. Mourguiart, 1995: Late Quaternary spatiotemporal limnological variations in the Altiplano of Bolivia and Peru. *Quat. Res.,* **43,** 344–354.
Wyrwoll, K.-H., and G. H. Miller, 2001: Initiation of the Australian summer monsoon 14,000 years ago. *Quat. Int.,* **83–85,** 119–128.
Yu, G., I. C. Prentice, S. P. Harrison, and X. Sun, 1998: Pollen-based biome reconstructions for China at 0ka and 6ka. *J. Biogeogr.,* **25,** 1055–1069.
——, S. P. Harrison, and B. Xue, 2001: Lake status records from China: Data base documentation. Tech. Rep. 4, Max-Planck-Institut fur biogeochemie, 50 pp.
Zhou, J., and K. M. Lau, 1998: Does a monsoon climate exist over South America? *J. Climate,* **11,** 1020–1040.